Computers and Geosciences 109 (2017) 258–267

Contents lists available at ScienceDirect

Computers and Geosciences

journal homepage: www.elsevier.com/locate/cageo

Research paper

Joint simulation of stationary grade and non-stationary rock type for quantifying geological uncertainty in a copper deposit

Mohammad Maleki [a,b], Xavier Emery [a,b,*]

[a] Department of Mining Engineering, University of Chile, Santiago, Chile
[b] Advanced Mining Technology Center, University of Chile, Santiago, Chile

ARTICLE INFO

Keywords:
Multigaussian model
Truncated Gaussian model
Intrinsic random fields of order *k*
Generalized covariance
Spectral simulation
Contact analysis
Semi-automated spatial structure identification

ABSTRACT

In mineral resources evaluation, the joint simulation of a quantitative variable, such as a metal grade, and a categorical variable, such as a rock type, is challenging when one wants to reproduce spatial trends of the rock type domains, a feature that makes a stationarity assumption questionable. To address this problem, this work presents methodological and practical proposals for jointly simulating a grade and a rock type, when the former is represented by the transform of a stationary Gaussian random field and the latter is obtained by truncating an intrinsic random field of order *k* with Gaussian generalized increments.

The proposals concern both the inference of the model parameters and the construction of realizations conditioned to existing data. The main difficulty is the identification of the spatial correlation structure, for which a semi-automated algorithm is designed, based on a least squares fitting of the data-to-data indicator covariances and grade-indicator cross-covariances. The proposed models and algorithms are applied to jointly simulate the copper grade and the rock type in a Chilean porphyry copper deposit. The results show their ability to reproduce the gradual transitions of the grade when crossing a rock type boundary, as well as the spatial zonation of the rock type.

1. Introduction

33333333The spatial distribution of the quantitative variables of interest in mineral resources evaluation is usually controlled by geological factors such as lithology, mineralization or alteration. When assessing the resources and the underlying uncertainty with geostatistical techniques, some dependence relationships between the random fields representing the quantitative variables and the controlling factors should therefore be taken into account. Most often, this is done with a hierarchical approach, by first partitioning the deposit into geological domains and, then, by simulating the quantitative variables within each domain (Roldão et al., 2012). As a result, the modeled variables exhibit clear-cut discontinuities when crossing the domain boundaries.

To avoid such discontinuities, one can consider the geological domains as a categorical covariate for the target quantitative variables. The former and the latter can then be jointly simulated by using Gaussian-based models (Dowd, 1997; Emery and Silva, 2009; Maleki and Emery, 2015). However, to date, most of these models rely on a stationarity hypothesis, which is unrealistic in the presence of spatial trends of the geological domains.

The solution proposed here is to look for a bivariate random field model, in which one random field (representing a quantitative variable, say, a metal grade) is stationary, while the other random field (representing the geological domains, say, rock type domains) is not stationary, but cross-correlated with the first one. In the following sections, we detail the process for inferring the model parameters (Section 2) and for constructing conditional realizations (Section 3). An application case study is presented in Section 4.

2. Joint modeling of grade and rock type

2.1. Grade modeling

Henceforth, we will consider a single metal grade, viewed as a realization of a stationary random field that can be monotonically transformed into a standard Gaussian random field. The model parameters are classically obtained by (1) transforming the grade data into normal scores, (2) calculating the experimental variogram or covariance of the normal scores, and (3) fitting a theoretical variogram or covariance model (Chilès and Delfiner, 2012). In the following, let us denote by Y_0 the stationary Gaussian random field associated with the transformed

* Corresponding author. Department of Mining Engineering, University of Chile, Santiago, Chile.
E-mail address: xemery@ing.uchile.cl (X. Emery).

http://dx.doi.org/10.1016/j.cageo.2017.08.015
Received 15 March 2017; Received in revised form 20 June 2017; Accepted 28 August 2017
Available online 31 August 2017
0098-3004/

grade and by K_0 its stationary covariance function.

2.2. Rock type modeling

Following Madani and Emery (2017), non-stationary rock type domains can be obtained by truncating an intrinsic random field of order k (IRF-k), hereafter denoted as Z, with Gaussian generalized increments and generalized covariance function K_1. For simplicity, a single IRF-k will be considered here, although the extension to several IRF-k is possible.

2.2.1. Finding a representation of the IRF-k with an ordinary covariance

To work with a random field that possesses an ordinary covariance function (and not only a generalized covariance), let us put

$$\forall \mathbf{x} \in \mathbb{R}^d, Y_1(\mathbf{x}) = Z(\mathbf{x}) - \mathbf{Z}_0^T \mathbf{\Lambda}(\mathbf{x}) \tag{1}$$

where d is the workspace dimension, $\mathbf{Z}_0$ is the $n \times 1$ vector with entry $Z(\mathbf{x}_i)$ at row i (with $\mathbf{x}_1 \ldots \mathbf{x}_n$ a set of given locations in $\mathbb{R}^d$) and $\mathbf{\Lambda}(\mathbf{x})$ is the $n \times 1$ vector containing the universal kriging weights $\lambda_1(\mathbf{x}) \ldots \lambda_n(\mathbf{x})$ assigned to $\mathbf{x}_1 \ldots \mathbf{x}_n$ when predicting location $\mathbf{x}$ with a pure nugget effect model and a polynomial drift of degree k. Let $\{f^l: l = 1 \ldots L\}$ be the basic drift functions (monomials of the spatial coordinates of degrees less than or equal to k), $\mathbf{F}_0$ the $L \times n$ matrix with $f^l(\mathbf{x}_i)$ as the entry at row l and column i, and $\mathbf{F}(\mathbf{x})$ the $L \times 1$ vector with entry $f^l(\mathbf{x})$ at row l. Then

$$\mathbf{\Lambda}(\mathbf{x}) = \mathbf{F}_0^T (\mathbf{F}_0 \mathbf{F}_0^T)^{-1} \mathbf{F}(\mathbf{x}) \tag{2}$$

The choice of the pure nugget effect model is merely instrumental, in order to provide a vector of weights $\mathbf{\Lambda}(\mathbf{x})$ that are linear combinations of the components of $\mathbf{F}(\mathbf{x})$, and does not presume the spatial structure of the random fields Y_1 and Z. Equation (1) becomes

$$\forall \mathbf{x} \in \mathbb{R}^d, Y_1(\mathbf{x}) = Z(\mathbf{x}) - \mathbf{Z}_0^T \mathbf{F}_0^T \left(\mathbf{F}_0 \mathbf{F}_0^T\right)^{-1} \mathbf{F}(\mathbf{x}) \tag{3}$$

The difference between $Y_1(\mathbf{x})$ and $Z(\mathbf{x})$ is a linear combination of the components of $\mathbf{F}(\mathbf{x})$, i.e., a polynomial function of the coordinates of $\mathbf{x}$. This implies that Y_1 is a representation of the same IRF-k as Z, insofar as an IRF-k is defined up to a polynomial of the coordinate of degree less than or equal to k (Chilès and Delfiner, 2012). Furthermore, since it coincides with a universal kriging error, $Y_1(\mathbf{x})$ is a generalized increment of Z and follows a Gaussian distribution with zero mean and finite variance. Accordingly, Y_1 is a Gaussian random field that possesses a covariance function C_1, which can be expressed as a function of the generalized covariance K_1:

$$\begin{aligned}\forall \mathbf{x},\mathbf{x}' \in \mathbb{R}^d, C_1(\mathbf{x},\mathbf{x}') = K_1(\mathbf{x}-\mathbf{x}') - \sum_{i=1}^{n} \lambda_i(\mathbf{x}) K_1(\mathbf{x}_i-\mathbf{x}) - \sum_{i=1}^{n} \lambda_i(\mathbf{x}') K_1(\mathbf{x}_i-\mathbf{x}') \\ + \sum_{i=1}^{n}\sum_{j=1}^{n} \lambda_i(\mathbf{x})\lambda_j(\mathbf{x}') K_1(\mathbf{x}_i-\mathbf{x}_j)\end{aligned} \tag{4}$$

According to Chilès and Delfiner (2012), the number of locations $\mathbf{x}_1 \ldots \mathbf{x}_n$ necessary to construct the representation Y_1 (hereafter called an "internal representation") should be such that

$$n \geq L = \frac{(k+d)!}{k!d!} \tag{5}$$

Let us standardize Y_1 by putting:

$$\forall \mathbf{x} \in \mathbb{R}^d, \tilde{Y}_1(\mathbf{x}) = \frac{Y_1(\mathbf{x})}{\sqrt{C_1(\mathbf{x},\mathbf{x})}} \tag{6}$$

which provides a Gaussian random field with zero mean, unit variance and non-stationary covariance function

$$\forall \mathbf{x}, \mathbf{x}' \in \mathbb{R}^d, \rho_1(\mathbf{x},\mathbf{x}') = \frac{C_1(\mathbf{x},\mathbf{x}')}{\sqrt{C_1(\mathbf{x},\mathbf{x}) C_1(\mathbf{x}',\mathbf{x}')}} \tag{7}$$

2.2.2. Truncating the representation of the IRF-k

Consider the indicator I_z obtained by truncating the original IRF-k at a threshold z:

$$\forall \mathbf{x} \in \mathbb{R}^d, I_z(\mathbf{x}) = \begin{cases} 1 \text{ if } Z(\mathbf{x}) < z \\ 0 \text{ otherwise} \end{cases} \tag{8}$$

This indicator can be rewritten as (Eqs. (3)–(7))

$$\forall \mathbf{x} \in \mathbb{R}^d, I_z(\mathbf{x}) = \begin{cases} 1 \text{ if } \tilde{Y}_1(\mathbf{x}) < y(\mathbf{x}) \\ 0 \text{ otherwise} \end{cases} \tag{9}$$

with

$$y(\mathbf{x}) = \frac{z - \mathbf{Z}_0^T \mathbf{F}_0^T (\mathbf{F}_0 \mathbf{F}_0^T)^{-1} \mathbf{F}(\mathbf{x})}{\sqrt{C_1(\mathbf{x},\mathbf{x})}} \tag{10}$$

The covariance function of I_z can be derived from that of the standard Gaussian random field $\widetilde{Y_1}$ (Chilès and Delfiner, 2012):

$$\begin{aligned}\forall \mathbf{x}, \mathbf{x}' \in \mathbb{R}^d, C_z(\mathbf{x},\mathbf{x}') \\ = g(y(\mathbf{x}))\, g(y(\mathbf{x}'))\, \sum_{p=1}^{+\infty} H_{p-1}(y(\mathbf{x}))\, H_{p-1}(y(\mathbf{x}'))\, \rho_1(\mathbf{x},\mathbf{x}')^p\end{aligned} \tag{11}$$

where $\{H_p: p \in \mathbb{N}\}$ are the Hermite polynomials and g is the standard Gaussian probability density function. Finally, the non-centered indicator covariance is:

$$\forall \mathbf{x}, \mathbf{x}' \in \mathbb{R}^d, E\{I_z(\mathbf{x}) I_z(\mathbf{x}')\} = C_z(\mathbf{x},\mathbf{x}') + G(y(\mathbf{x}))\, G(y(\mathbf{x}')) \tag{12}$$

where G is the standard Gaussian cumulative distribution function. The right-hand side is a function of the known locations and weights used to construct the internal representation Y_1, and of the unknown generalized covariance K_1, threshold z and vector $\mathbf{Z}_0$ (involved in the definition of $y(\mathbf{x})$ in Equation (10)). Concerning the left-hand side, an experimental estimate can be computed for each pair of data locations where I_z is known. Therefore, if one assumes a parametric form for K_1 (e.g., a weighted sum of known nested models with unknown weights), one can estimate K_1, z and $\mathbf{Z}_0$ so as to minimize the sum of squared errors between the experimental and theoretical covariances (Eq. (12)) (Madani and Emery, 2017).

2.3. Modeling the cross-correlation between grade and rock type

Let K_{10} be the generalized cross-covariance between the IRF-k modeling the rock type domains (Z) and the stationary Gaussian random field modeling the grade (Y_0). The cross-covariance between Y_0 and the internal representation Y_1 can be expressed as:

$$\begin{aligned}\forall \mathbf{x}, \mathbf{x}' \in \mathbb{R}^d, C_{10}(\mathbf{x},\mathbf{x}') := \operatorname{cov}\{Y_1(\mathbf{x}), Y_0(\mathbf{x}')\} \\ = \operatorname{cov}\left\{ Z(\mathbf{x}) - \sum_{i=1}^{n} \lambda_i(\mathbf{x}) Z(\mathbf{x}_i), Y_0(\mathbf{x}') \right\} \\ = K_{10}(\mathbf{x}-\mathbf{x}') - \sum_{i=1}^{n} \lambda_i(\mathbf{x}) K_{10}(\mathbf{x}_i-\mathbf{x}')\end{aligned} \tag{13}$$

The cross-covariance between the standardized representation $\widetilde{Y_1}$ and Y_0 is:

$$\forall \mathbf{x}, \mathbf{x}' \in \mathbb{R}^d, \rho_{10}(\mathbf{x},\mathbf{x}') := \operatorname{cov}\{\tilde{Y}_1(\mathbf{x}), Y_0(\mathbf{x}')\} = \frac{C_{10}(\mathbf{x},\mathbf{x}')}{\sqrt{C_1(\mathbf{x},\mathbf{x})}} \tag{14}$$

To determine the cross-covariance between Y_0 and the indicator I_z defined in Equations (8) and (9), let us expand the indicator into Hermite

polynomials:

$$\forall \mathbf{x},\mathbf{x}' \in \mathbb{R}^d, C_{z,0}(\mathbf{x},\mathbf{x}') := \mathrm{cov}\left\{1_{\tilde{Y}_1}(\mathbf{x}) < y(\mathbf{x}), Y_0(\mathbf{x}')\right\} = \mathrm{cov}\left\{G(y(\mathbf{x})) + \sum_{p=1}^{+\infty} \frac{1}{\sqrt{p}} H_{p-1}(y(\mathbf{x}))g(y(\mathbf{x}))H_p(\tilde{Y}_1(\mathbf{x})), Y_0(\mathbf{x}')\right\} \quad (15)$$

On the one hand, one has:

$$Y_0(\mathbf{x}') = -H_1(Y_0(\mathbf{x}')) \quad (16)$$

On the other hand, as the Hermite polynomials applied to jointly standard Gaussian random fields do not have any cross-correlation unless they have the same degree, one obtains:

$$C_{z,0}(\mathbf{x},\mathbf{x}') = -g(y(\mathbf{x}))\mathrm{cov}\left\{\tilde{Y}_1(\mathbf{x}), Y_0(\mathbf{x}')\right\} = -g(y(\mathbf{x}))\rho_{10}(\mathbf{x},\mathbf{x}') \quad (17)$$

The right-hand side is a function of the known locations and weights used to construct the internal representation Y_1, and of the unknown generalized cross-covariance K_{10}, threshold z and vector $\mathbf{Z}_0$. As for the left-hand side, an experimental estimate can be computed for each pair of data locations where I_z and Y_0 are known. Therefore, if one assumes a parametric form for K_{10}, one can estimate K_{10}, z and $\mathbf{Z}_0$ so as to minimize the sum of squared errors between the experimental and theoretical cross-covariances (Eq. (17)).

2.4. Joint modeling of the correlation structure of grade and rock type

As they involve common parameters (threshold z and vector $\mathbf{Z}_0$), the inference of the rock type model (generalized covariance K_1) and of the cross-correlation (generalized cross-covariance K_{10}) should be performed in a single least squares fitting process. In summary, the steps to infer both the generalized direct and cross-covariances are:

- Choice of model parameters:
  - an order k for the IRF-k Z representing the rock type;
  - a set of locations $\mathbf{x}_1 \ldots \mathbf{x}_n$ on which to construct the representation Y_1;
  - a set of basic nested structures for the direct and cross-covariances K_0, K_1 and K_{10}. The unknowns can be the sills, slopes, exponents, shape parameters and scale parameters of these nested structures.
- Experimentally calculate the data-to-data indicator covariance matrix, as well as the data-to-data indicator-normal scores cross-covariance matrix.
- Calculate the theoretical data-to-data indicator covariance matrix (Eq. (12)) and data-to-data indicator-normal scores cross-covariance matrix (Eq. (17)), which depend on the parameters to be fitted.
- Find the covariance parameters, threshold z and vector $\mathbf{Z}_0$ that minimize the sum of squared errors between the experimental and theoretical direct covariance and cross-covariance matrices. A trust region algorithm (Yuan, 2015) can be used for this purpose.

$\mathbf{Z}_0$ varies from one realization to another, as it depends on the values of the representation of the intrinsic random field Z at the chosen locations $\mathbf{x}_1 \ldots \mathbf{x}_n$, while the parameters of the generalized direct covariance K_1 and cross-covariance K_{10} remain the same for all the realizations of this intrinsic random field. Therefore, one should keep only the latter parameters for the simulation stage, not the value of $\mathbf{Z}_0$ delivered by the least-squares fitting algorithm.

Also, because z and $\mathbf{Z}_0$ are fitted through the difference $z - \mathbf{Z}_0^T\mathbf{F}_0^T(\mathbf{F}_0\mathbf{F}_0^T)^{-1}\mathbf{F}(\mathbf{x})$ that defines the numerator of the ratio in Equation (10), the exact value of z remains undetermined. This indetermination is actually not an issue: instead of truncating the initial representation Z at threshold z (Eq. (8)), one can use another representation of the same IRF-k equal to $Z - z$ with a truncation threshold equal to zero. In other words, up to a change in the representation of the IRF-k, the truncation threshold z can be set to zero without loss of generality.

2.5. An example of bivariate covariance model

Suppose that K_1 is a power covariance with slope c_1 and exponent α_1, and that K_0 and K_{10} are Matérn covariance functions with sills c_0 and c_{10} and shape parameters μ_0 and μ_{10}, respectively. The Matérn covariance is chosen here because of its versatility, as the shape parameter controls its behavior at the origin. In this section, all these covariances are further assumed to have a unit scale parameter, but this parameter can be modified to any other value, possibly depending on the direction in case of anisotropy.

The matrix of generalized direct and cross-covariances is:

$$\mathbf{C}(\mathbf{h}) = \begin{pmatrix} K_0(\mathbf{h}) & K_{10}(\mathbf{h}) \\ K_{10}(\mathbf{h}) & K_1(\mathbf{h}) \end{pmatrix} \quad (18)$$

The corresponding spectral density matrix is:

$$\mathbf{f}(\boldsymbol{\omega}) = \begin{pmatrix} f_0(\boldsymbol{\omega}) & f_{10}(\boldsymbol{\omega}) \\ f_{10}(\boldsymbol{\omega}) & f_1(\boldsymbol{\omega}) \end{pmatrix} \quad (19)$$

where f_0, f_1 and f_{10} are the spectral densities of the Matérn direct covariance, power direct covariance and Matérn cross-covariance, respectively, i.e. (Lantuéjoul, 2002; Chilès and Delfiner, 2012):

$$\begin{aligned} f_0(\boldsymbol{\omega}) &= c_0\frac{\Gamma(\mu_0 + d/2)}{\Gamma(\mu_0)\pi^{d/2}} \frac{1}{\left(1 + ||\boldsymbol{\omega}||^2\right)^{\mu_0+d/2}} \\ f_1(\boldsymbol{\omega}) &= c_1\frac{\Gamma(\alpha_1/2+1)\Gamma(\alpha_1/2+d/2)}{\Gamma(\alpha_1/2-k)\Gamma(1-\alpha_1/2+k)\pi^{\alpha_1+d/2}} \frac{1}{(2\pi)^d(||\boldsymbol{\omega}||/(2\pi))^{\alpha_1+d}} \\ f_{10}(\boldsymbol{\omega}) &= c_{10}\frac{\Gamma(\mu_{10} + d/2)}{\Gamma(\mu_{10})\pi^{d/2}} \frac{1}{\left(1 + ||\boldsymbol{\omega}||^2\right)^{\mu_{10}+d/2}} \end{aligned} \quad (20)$$

with k the integer part of $\alpha_1/2$. To have an admissible model, $\mathbf{f}(\boldsymbol{\omega})$ must be positive semi-definite for any $\boldsymbol{\omega}$ (Chilès and Delfiner, 2012), i.e.:

$$\forall \boldsymbol{\omega} \in \mathbb{R}^d, f_0(\boldsymbol{\omega})f_1(\boldsymbol{\omega}) \geq f_{10}^2(\boldsymbol{\omega}) \quad (21)$$

After simplification, one obtains the following two constraints.

- First constraint

$$4\mu_{10} - 2\mu_0 \geq \alpha_1 \quad (22)$$

- Second constraint

$$c_{10}^2 \leq c_0c_1\frac{\Gamma(\mu_0 + d/2)\Gamma(\alpha_1/2+1)\Gamma(\alpha_1/2+d/2)\Gamma^2(\mu_{10})2^{\alpha_1}}{\Gamma(\mu_0)\Gamma(\alpha_1/2-k)\Gamma(1-\alpha_1/2+k)\Gamma^2(\mu_{10}+d/2)} \quad (23)$$

In a nutshell, by considering Equations (22) and (23), one needs to find suitable covariance parameters (c_0, c_1, c_{10}, μ_0, μ_{10}, α_1). The

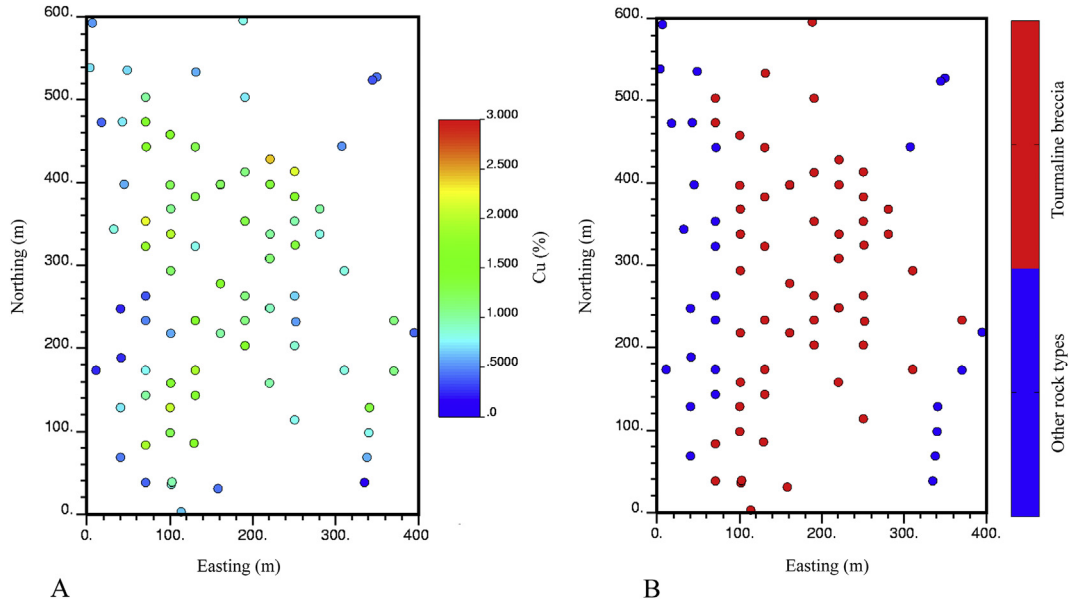

Fig. 1. Location maps of copper grade (A) and rock type (B) data (plan view of drill hole data with elevations between 94 m and 106 m).

parameters associated with the grade (c_0 and μ_0) can be fitted directly on the basis of the experimental variogram or covariance of the normal scores data, while the remaining parameters should be fitted by least squares optimization based on Equations (12) and (17).

3. Joint simulation of grade and rock type

3.1. Non-conditional simulation

Having determined the model parameters, one can jointly simulate the two random fields Y_0 and Z with an algorithm based on the spectral representation of the generalized covariance functions. Specifically, let us define a vector random field with two scalar components as follows:

$$\forall \mathbf{x} \in \mathbb{R}^d, \mathbf{Y}(\mathbf{x}) = \sum_{p=1}^{2} \alpha_p(\boldsymbol{\omega}_p)\cos\left(2\pi < \mathbf{x} | \boldsymbol{\omega}_p > + \phi_p\right) \quad (24)$$

where $< | >$ represents the dot product in $\mathbb{R}^d$

$\{\boldsymbol{\omega}_p: p = 1, 2\}$ are independent random vectors with probability density h in $\mathbb{R}^d$
$\{\phi_p: p = 1, 2\}$ are independent random variables uniform on $[0,2\pi]$
$\{\alpha_p: p = 1, 2\}$ are vector-valued mappings with two real-valued components.

For the random field $\mathbf{Y}$ to have (generalized) direct and cross-covariances associated with the target spectral density matrix $\mathbf{f}$, the following condition must be satisfied (Emery et al., 2016; Arroyo and Emery, 2016):

$$\mathbf{A}(\boldsymbol{\omega})\mathbf{A}(\boldsymbol{\omega})^T = \frac{2\mathbf{f}(\boldsymbol{\omega})}{h(\boldsymbol{\omega})} \quad (25)$$

where $\mathbf{A}(\boldsymbol{\omega})$ is the 2×2 matrix whose p-th column is $\alpha_p(\boldsymbol{\omega})$. The necessary conditions to find a matrix $\mathbf{A}(\boldsymbol{\omega})$ fulfilling the above equation are that $\mathbf{f}(\boldsymbol{\omega})$ is a real-valued symmetric positive semi-definite matrix for any $\boldsymbol{\omega} \in \mathbb{R}^d$ and that the support of h contains the support of $\mathbf{f}$. In such a case, $\mathbf{A}(\boldsymbol{\omega})$ can be obtained by taking the Cholesky factor of $2\mathbf{f}(\boldsymbol{\omega})/h(\boldsymbol{\omega})$.

To obtain a random field with (approximately) multivariate-Gaussian increments, it suffices to sum up and normalize many of such independent random fields (Arroyo and Emery, 2016):

$$\forall \mathbf{x} \in \mathbb{R}^d, \mathbf{Y}(\mathbf{x}) = \frac{1}{\sqrt{Q}} \sum_{q=1}^{Q} \mathbf{Y}_q(\mathbf{x}) \quad (26)$$

where Q is a large integer and $\{\mathbf{Y}_q: q = 1 \ldots Q\}$ are mutually independent random fields defined as in Equation (24).

Given a fixed number Q of basic random fields, the computational cost (in terms of floating points operations) for calculating R realizations of $\mathbf{Y}(\mathbf{x})$ at N locations in $\mathbb{R}^d$ is $O(N{\cdot}R)$, i.e., proportional to N and R. For comparison, sequential simulation requires between $O(N^3{\cdot}R)$ and $O(N^4{\cdot}R)$ operations (Dimitrakopoulos and Luo, 2004), while spectral approaches based on fast Fourier transforms require $O(N{\cdot}\ln(N){\cdot}R)$ operations (Gneiting et al., 2006; Liang et al., 2016). For large N, the computational requirement of our spectral algorithm is therefore significantly lower and is comparable to that of the more general turning bands algorithm (Lantuéjoul, 2002). Calculations can be parallelized by recourse to multi-core processors and/or GPU computing.

Another advantage of this algorithm relates to its minimal memory requirement, insofar as the values simulated at every location can be stored in an output file without waiting for the simulation at any other location. In contrast, sequential and discrete spectral simulations often require keeping in memory all the simulated values in each realization ($2{\cdot}N$ values in the present case) before writing them in the output file (Liang et al., 2016).

3.2. Conditioning to data

In the stationary case, one can convert a non-conditional simulation into a conditional one thanks to an additional step based on simple kriging or cokriging. In the present case however, one random field (Y_0) is stationary, but the other one (Z) is not. Accordingly, simple cokriging can no longer be used to condition the realizations.

To obtain conditional realizations of both random fields, a specific version of cokriging (mixed simple/intrinsic cokriging) has to be used, which accounts for the stationarity and known mean value of the first random field and the non-stationarity of the second one. The elements of the right-hand and left-hand side kriging matrices are filled by considering the generalized direct and cross-covariances and the basic drift functions associated with the non-stationary random field.

This specific version of cokriging should actually be used not only for conditioning the realizations, but also in the Gibbs sampler required in

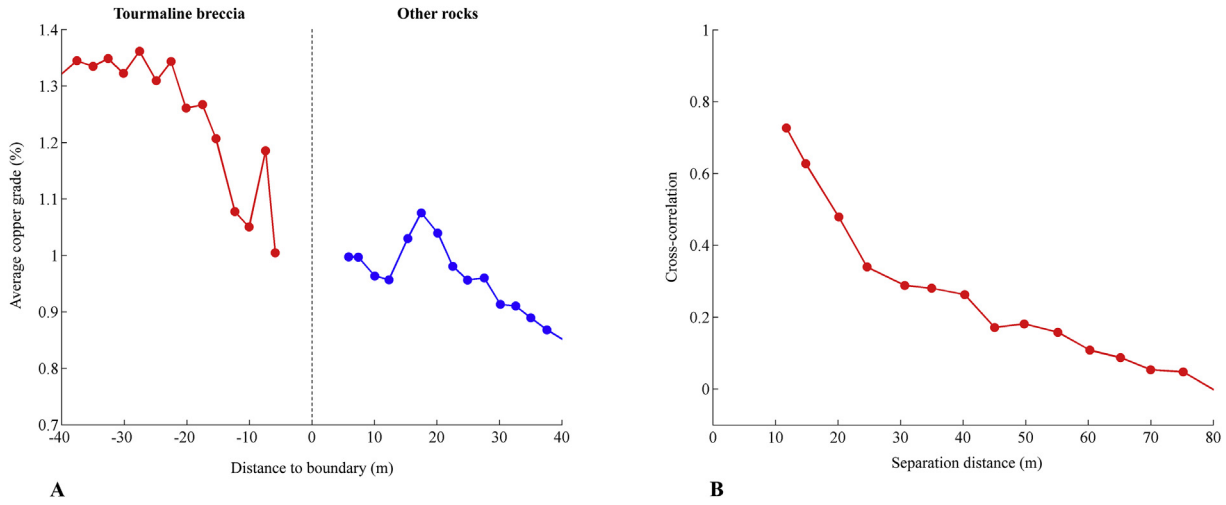

Fig. 2. Contact analysis of drill hole data: A) mean grade graph and B) correlation graph.

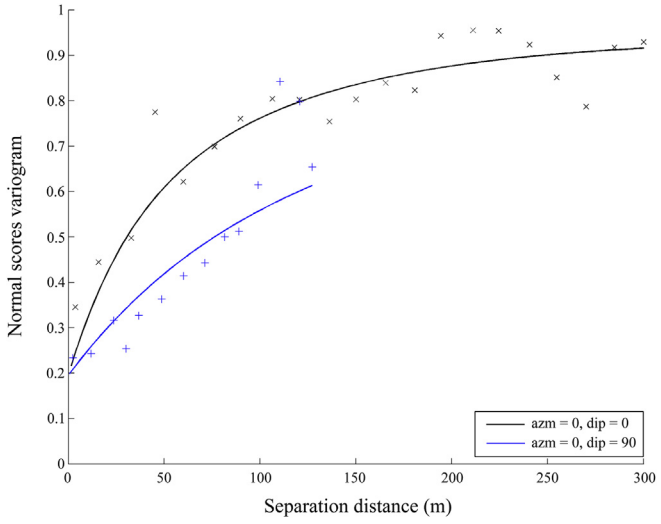

Fig. 3. Sample (crosses) and modeled (solid lines) variograms along main anisotropy directions (transformed copper grade).

the truncated Gaussian algorithm for constructing Gaussian data from known data on the rock type domains (Armstrong et al., 2011).

4. Case study

4.1. Presentation of data and exploratory analysis

The models and algorithms presented in the previous sections are now applied to a case study in mineral resources evaluation. The available data consist of 737 samples from exploration drill holes in a region of size 400 m × 600 m × 130 m belonging to the Río Blanco - Los Bronces porphyry copper deposit (Chilean Central Andes), with information on the rock types and total copper grades (Fig. 1). Two main rock types that control the copper grade distribution can be distinguished (Frikken, 2003):

- High-graded tourmaline breccia: the matrix is a milled rock flour with biotite and tourmaline cement and open spaces filled by tourmaline-quartz-sulfide.
- Other rocks, which include granodiorite and diorite whose mineralogy is composed of plagioclase, orthoclase, quartz, biotite and hornblende, as well as low-graded breccias with a matrix of milled rock flour and low proportion of tourmaline.

From Fig. 1, one observes a clear zonation, where the tourmaline breccia is present only in the central part of the region, while the lateral parts on the eastern and western sides are covered by the other rock types. A stationary modeling of the rock type would therefore be questionable. Instead, a non-stationary model will be used, based on the truncation of an IRF-*k*.

4.2. Contact analysis

To know whether or not a joint simulation approach is suited for this case study, a contact analysis is carried out to determine the behavior of the copper grade in the neighborhood of the boundary between the two rock types (Maleki and Emery, 2015). In particular, the mean copper grade in the other rocks appears to be rather continuous across the boundary with the nearby mean copper grade of the breccia (Fig. 2A). Also, the cross-correlation between a copper grade data located in the breccia and a copper grade data located in the other rocks turns out to be high (greater than 0.6) when the distance separating the two data locations is less than 15 m, and slowly decays to zero as the separation distance increases (Fig. 2B). These results suggest a soft contact and incite us to use the proposed joint simulation method instead of the conventional hierarchical approach. Note that the representations in Fig. 2A and B omit the statistics associated with the short distances, which actually involve very few data (less than 5, against several tens or hundreds data for the remaining distances) and are therefore not robust.

4.3. Spatial structure analysis

4.3.1. Structural analysis of copper grade

To identify the spatial structure of the stationary Gaussian random field Y_0, the grade data are transformed into normal scores and variogram analysis is performed on the normal scores. The experimental variogram is calculated along the vertical and horizontal directions. The fitted model (generalized covariance K_0) comprises a nugget effect and two nested Matérn structures with shape parameters equal to 0.5, which correspond to exponential models (Fig. 3):

$$K_0 = 0.19\,nugget + 0.29\,Matérn_{0.5}(30m, 75m) + 0.45\,Matérn_{0.5}(100m, 250m) \quad (27)$$

The distances into brackets indicate the scale parameters along the horizontal and vertical directions, respectively, while the scalar

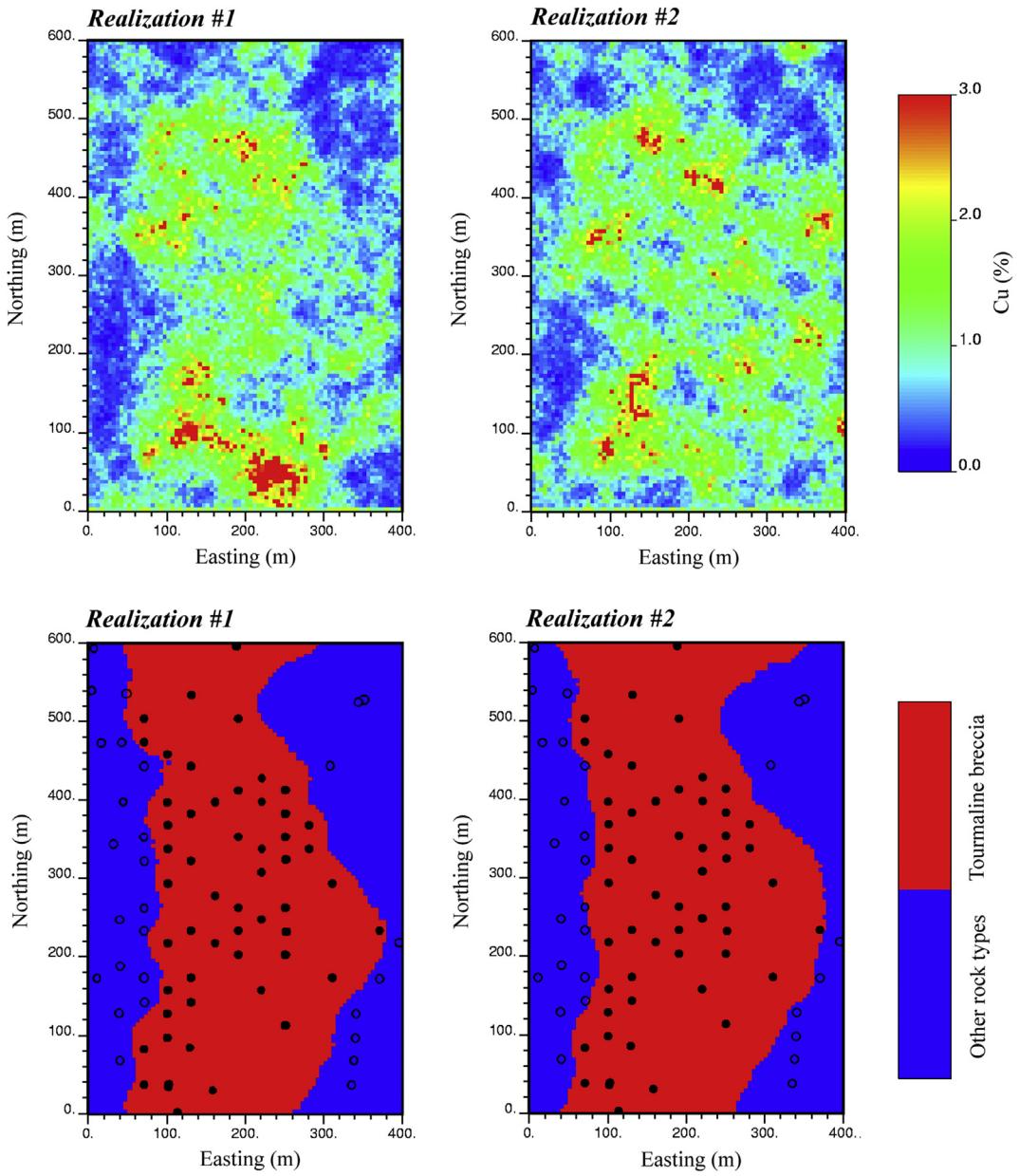

Fig. 4. Two conditional realizations of the copper grade and rock type (plan view with elevation 100 m). The rock type of drill hole data between elevations 94 m and 106 m has been superimposed, with filled and unfilled circles to indicate the belonging to tourmaline breccia and other rock types, respectively.

coefficient before each structure indicates the sill of this structure.

4.3.2. Joint structural analysis of copper grade and rock type

We suppose that the rock type indicator is obtained by truncating an IRF-k, denoted as Z. The spatial structure of Y_0 and Z, i.e., their generalized direct and cross-covariances, can be determined with the methodology presented in Section 2, which relies on the choice of:

(1) an order k for the intrinsic random field Z;
(2) a set of locations for constructing an internal representation of Z;
(3) a set of basic nested structures for the direct (K_0 and K_1) and cross (K_{10}) covariance models.

In relation to the intrinsic random field, let us consider an order $k = 1$ that allows for a drift that can account for the rock type zonation. The minimal number of locations needed to construct an internal representation is $n = 4$ (Eq. (5)); these locations are chosen randomly over the region of interest. More locations could be considered in order to get a more robust representation of the drift, but this would increase the number of parameters (size of vector $\mathbf{Z}_0$) and make the semi-automated fitting process more complex.

Concerning the nested structures, the direct covariance K_0 of the Gaussian random field Y_0 has been fitted in the previous subsection with a nugget effect and two Matérn structures (Eq. (27)). Under these conditions, let us assume a bivariate model for K_0, K_1 and K_{10} composed of two structures (apart from the nugget effect).

The first structure is a model where all the generalized direct and cross-covariances are Matérn covariances. For the sake of simplicity, we will set the shape and scale parameters along the horizontal and vertical directions to the same values as that found in the fitting of K_0, i.e. a shape parameter equal to 0.5 and scale parameters equal to 30 m (horizontally) and 75 m (vertically). This bivariate model boils down to an intrinsic correlation model where the generalized direct and cross-covariances are proportional to the same exponential covariance.

The second structure is a bivariate model where the generalized direct covariance associated with the rock type is a power model and the

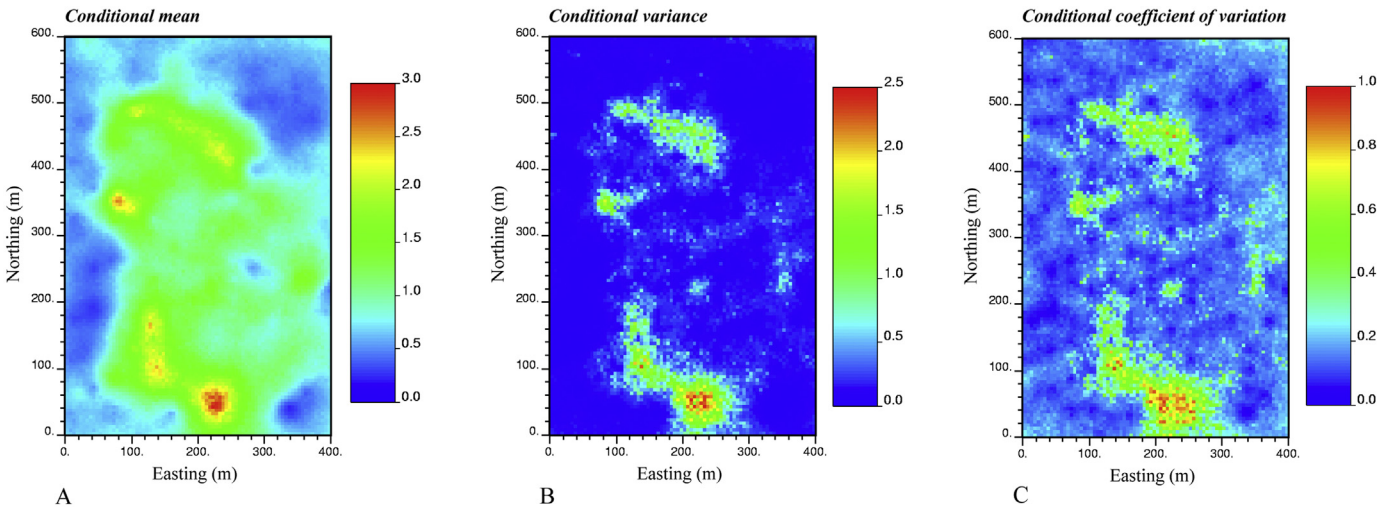

Fig. 5. A) Conditional mean, B) conditional variance and C) conditional coefficient of variation (plan view with elevation 100 m) for the joint simulation approach.

other direct and cross-covariances are Matérn, as presented in Section 2.5. Again, some choices are necessary to reduce the number of parameters to be fitted by the least-squares algorithm presented in Section 2.4. One can fix the exponent, shape and scale parameters of this bivariate model and leave only the sills or slope to the least-squares fitting:

- *Scale parameters*: the same scale parameters as the ones found when fitting K_0 will be used, so as to preserve the anisotropy directions and anisotropy ratio of the grade model.
- *Exponent*: to obtain an IRF-1 for Z, the exponent of its power covariance should be between 2 and 4 (Chilès and Delfiner, 2012). For simplicity, we chose a value of 3.
- *Shape parameter*: the lower bound for the shape parameter of the cross-covariance between Y_0 and Z is 1, as per Equation (22). Again, for simplicity, we will take this bound as the parameter value.

The generalized direct and cross-covariances of the random fields Y_0 and Z will therefore be assumed of the following form:

$$\begin{cases} K_0 = 0.19nugget + 0.29Matérn_{0.5}(30m, 75m) + 0.45Matérn_{0.5}(100m, 250m) \\ K_1 = c_1 Matérn_{0.5}(30m, 75m) + c_1' Power_3(100m, 250m) \\ K_{10} = c_{10} Matérn_{0.5}(30m, 75m) + c_{10}' Matérn_1(100m, 250m) \end{cases} \quad (28)$$

The coefficients c_1, c_1', c_{10} and c_{10}' are fitted by the least-squares algorithm presented in Section 2.4, which aims to obtain the smallest total sums of squared errors between the experimental and modeled covariance matrices of the indicator data and cross-covariance matrices of indicator and normal scores data. One finds

$$c_1 = 0.030, c_1' = 0.098, c_{10} = 0 \text{ and } c_{10}' = 0.252 \quad (29)$$

These coefficients fulfill the condition in Equation (23) to be mathematically valid.

Due to the Matérn structure, the generalized covariance K_1 is linear at the origin, which produces irregular boundaries between the two rock types when truncating the IRF-1 (Lantuéjoul, 2002). However, the Matérn structure becomes negligible in comparison with the power structure for distances greater than 30 m, so that the irregular behavior of the rock type boundaries will convert into a smoother behavior at the scale of a few tens of meters, which agrees with the geological understanding of the deposit and with the map in Fig. 1B.

4.4. Conditional simulation

Provided with the spatial correlation model, one can construct realizations of the grade and rock type. The simulation first consists in simulating the intrinsic random field Z at the drill hole data locations, conditionally to the grade and rock type data, by Gibbs sampling (using mixed simple/intrinsic cokriging for determining the successive conditional distributions, as indicated in Section 3.2). Cokriging is implemented in a unique neighborhood, which theoretically ensures the convergence of the Gibbs sampler (Emery et al., 2014), and the Gibbs sampler is stopped after 10,000 iterations, i.e., when the value at each drill hole data has been updated 10,000 times; such a number of updates is chosen to obtain a good match in the reproduction of the spatial correlation structure, as suggested in Emery et al. (2014). The spectral algorithm is then applied to construct non-conditional realizations at the data locations and over the region of interest, discretized by a regular grid with a spacing of 5 m × 5 m × 12 m along the east, north and elevation coordinates, respectively. One thousand (Q = 1 000) basic random fields are used at this stage (Eq. (26)). The realizations are subsequently conditioned to the data (normal scores data for grade and output of the Gibbs sampler for rock type), again by using mixed simple/intrinsic cokriging.

One hundred realizations are generated, two of which are displayed in Fig. 4. As expected, no discontinuity is observed in the copper grade when crossing the boundary between the two rock types (soft boundaries). The maps are consistent with the data values shown in Fig. 1, where the tourmaline breccia is located in the center of the region under study and contains the highest copper grade.

4.5. Post-processing the realizations

Fig. 5 displays the conditional mean, identified as the average of the realizations, conditional variance (CV) and conditional coefficient of variation (CCV) of the copper grade. Both the CV and CCV measure the uncertainty in the true (unknown) copper grade and reflect a

proportional effect (higher uncertainty in high-graded areas).

One can also calculate the uncertainty in the rock type at each target grid node, through a probability map (Fig. 6). As can be seen from this map, the probability of occurrence of tourmaline breccia is very high in the center of the region under study and almost zero in the eastern and western sides. This zonation is consistent with the drill hole data and with the geological understanding of the deposit.

4.6. Validation against blast hole data

The identification of the spatial structure in Section 4.3.2 depends on several subjective decisions of the modeler, in particular, the choice of the order for the random field Z, of the number and coordinates of the locations used for constructing the internal representation, of the number and types of basic nested structures and of some of their parameters (exponents, scale and shape parameters). From the authors' experience, the resulting model is sensitive to all these decisions and so are the simulation results. An important step is therefore the validation of the fitted generalized direct and cross-covariances, which can be done by the leave-one-out cross-validation or the split-sample method.

Here, a validation against 20,893 blast hole data is done, by simulating the copper grade at the blast hole locations (Fig. 7A) and comparing the simulated values with the true values. On the one hand, Fig. 7B shows the scatter plot of the average of 100 copper grade realizations versus the true copper grades measured at the blast hole samples, which indicates that the average simulated values are unbiased (mean error equal to −0.013), conditionally unbiased (regression line close to the bisector) and precise (scatter plot with little dispersion around the bisector, reflected by a mean squared error equal to 0.350). On the other hand, from the conditional realizations, one can also compute a series of symmetric probability intervals (PI) at each blast hole location. The bounds of the PI of probability p are the quantiles $(1–p)/2$ and $(1+p)/2$ of the distribution of simulated values. A correct modeling of the grade uncertainty would entail that a proportion p of the probability intervals contains the true copper grade value (Goovaerts, 2001). As a consequence, the scatter plot of the probability p versus the proportion of blast hole data contained in the p-PI (known as an accuracy plot) allows visualizing the match between observed and expected proportions as a function of p. This plot (Fig. 7C) indicates an accurate modeling of the uncertainty, as the departures from the identity line are small.

The blast hole data do not carry information on the rock type, but a validation of the rock type model has been made in the previous section, by comparing the probability map (Fig. 6) in the light of the geological knowledge of the deposit.

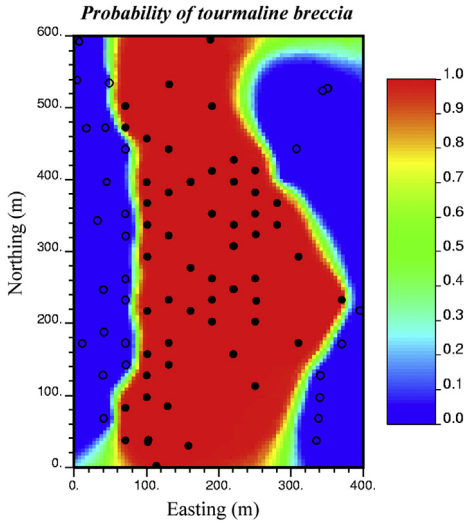

Fig. 6. Conditional probability of tourmaline breccia (plan view with elevation 100 m). The rock type of drill hole data between elevations 94 m and 106 m has been superimposed, with filled and unfilled circles to indicate the belonging to tourmaline breccia and other rock types, respectively.

4.7. Comparison with the hierarchical approach

For comparison, let us simulate the rock type and the copper grade in a hierarchical way. For the rock type simulation, the same procedure as for the joint simulation is used, except that all the copper grade data are removed and only the rock type data are kept. This amounts to constructing 100 realizations of an IRF-1 with generalized covariance K_1 (Eqs. (28) and (29)) at the data locations, conditioned to the rock type information at these locations, by Gibbs sampling. Then, 100 non-conditional realizations are generated at the data locations and target grid nodes by the spectral algorithm and converted into conditional realizations with intrinsic kriging, using the Gibbs sampler output. As for the copper grade simulation, the following steps are used for each rock type (tourmaline breccia and other rocks):

1 Transform the copper grade data into normal scores
2 Calculate the experimental variogram of the normal scores
3 Fit a theoretical (stationary) variogram model
4 For each rock type realization:

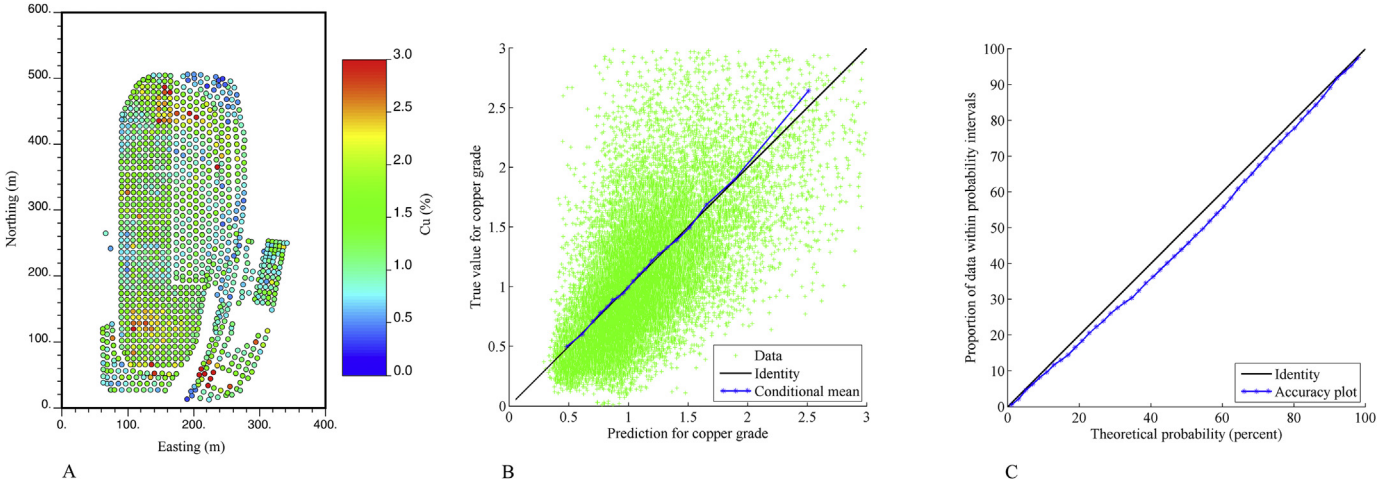

Fig. 7. Split-sample validation of the simulated copper grades: A, map of blast hole data (plan view with elevation 100 m); B, scatter plot between true copper grades and average of 100 realizations; C, accuracy plot comparing the proportion of blast hole data within PI-intervals against the nominal interval probability.

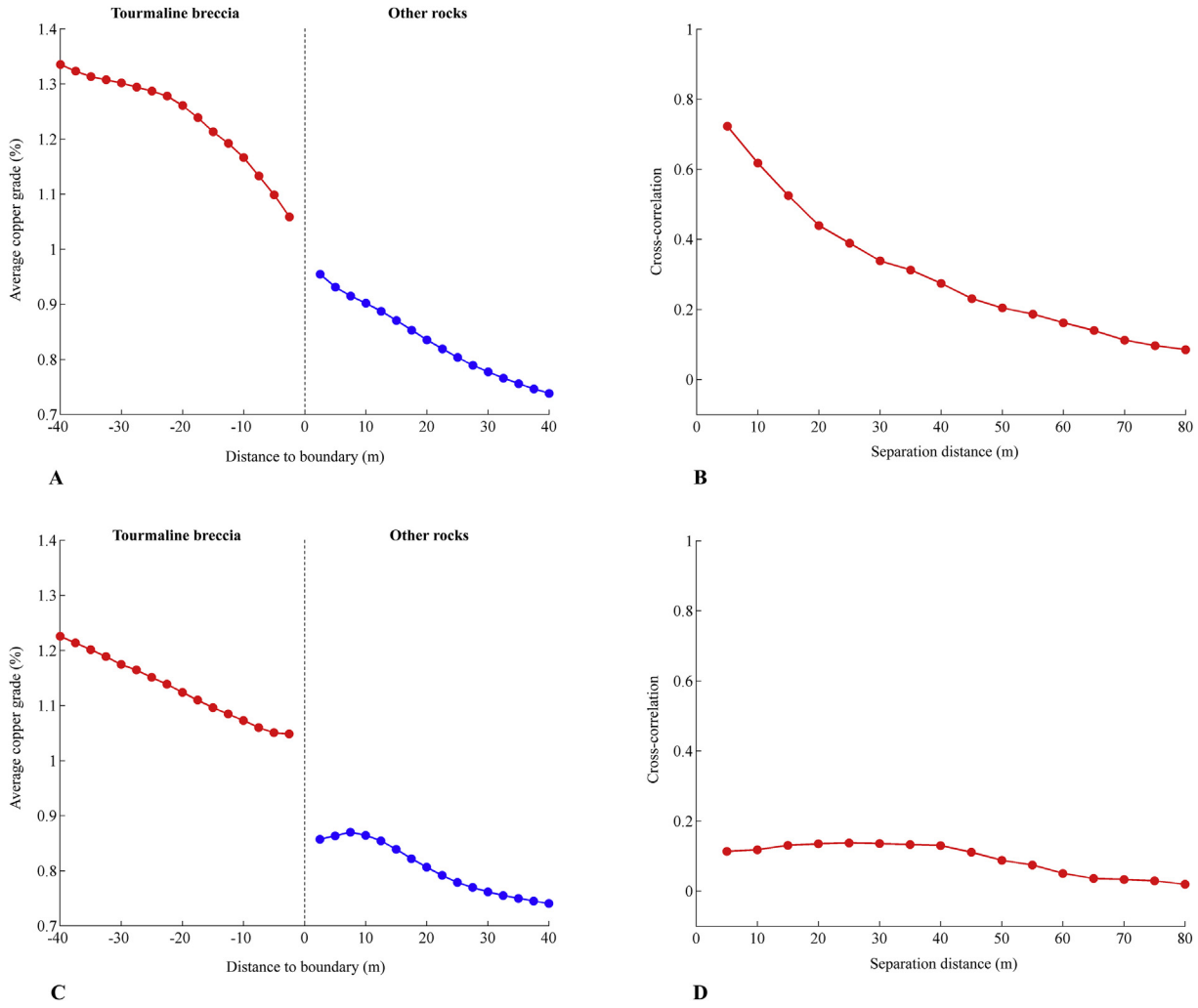

Fig. 8. Contact analysis mean grade graphs (A, C) and correlation graphs (B, D) for joint (A, B) and hierarchical (C, D) simulation at the target grid nodes (first realization).

- Construct a non-conditional realization of the transformed grade at the locations belonging to this rock type, using a spectral algorithm (Emery et al., 2016).
- Condition the realization to the normal scores by simple kriging.
- Back-transform the simulated values from the Gaussian scale to the grade scale.

This way, one obtains as many copper grade realizations as rock type realizations (100). The results of this approach are compared with the ones obtained with the joint simulation approach.

4.7.1. *Reproducing the nature of the rock type boundary*

A contact analysis is carried out to determine the behavior of the

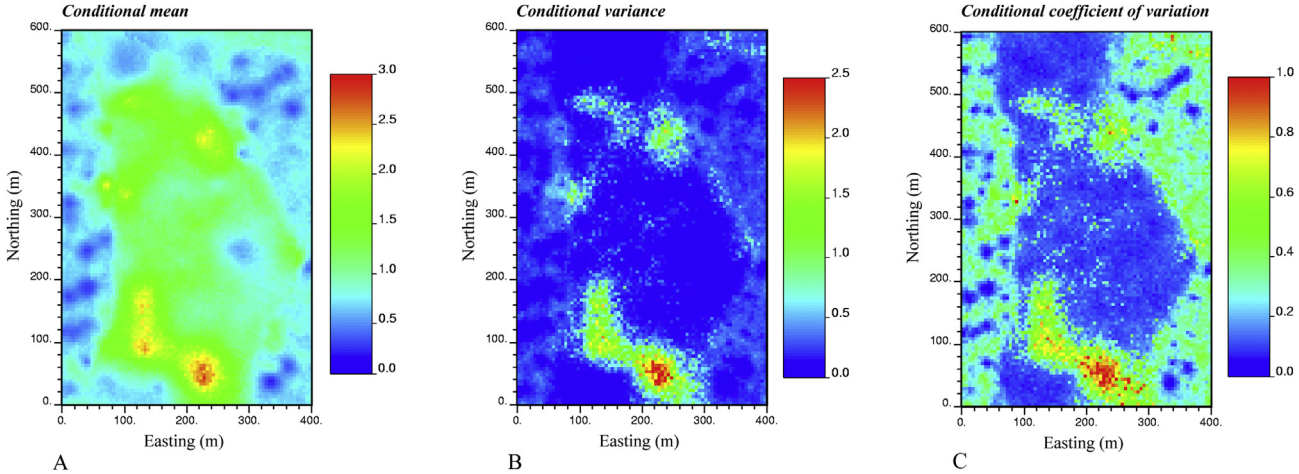

Fig. 9. A) Conditional mean, B) conditional variance and C) conditional coefficient of variation for the hierarchical approach (plan view with elevation 100 m).

simulated copper grade near the rock type boundary. Regarding the joint simulation approach, it is seen that the mean grade exhibits a gradual transition when crossing the rock type boundary (Fig. 8A) and that the simulated grades are correlated across the boundary (Fig. 8B), similarly as what is observed in the original data (Fig. 2). This corroborates that the joint simulation approach reproduces the soft boundary between rock types. Conversely, the analysis related to the hierarchical approach (Fig. 8C and D) indicates a discontinuity in the mean values and a weak correlation of the simulated copper grades when crossing the boundary. This is explained because the hierarchical model neglects the spatial correlation of the copper grade across the boundary and therefore produces a hard boundary.

4.7.2. Prediction of copper grades

The conditional mean grade obtained with the hierarchical approach (Fig. 9A) is higher in the edges of the region under study in comparison with the joint simulation approach (Fig. 5A). This can be explained because, in the joint simulation, the copper grade is positively correlated with the IRF-1 associated with the rock type, which is likely to take large negative values in the outer locations. In contrast, in the hierarchical approach, the prior mean grade is constant in each rock type, so the variations in the conditional mean are only due to the effect of the conditioning data (these data are not abundant in the other rock type, so their effect is moderate).

4.7.3. Quantification of grade uncertainty

As seen in Figs. 5 and 9, both the CV and CCV are significantly higher when using the hierarchical approach, which is explained because this approach uses fewer conditioning data when simulating the grades in each rock type (tourmaline breccia data are neglected when simulating the other rock types, and vice-versa, which leads to a greater uncertainty). As a result, if one uses these measures for classifying the mineral resources, the amount of measured ore tonnage is likely to increase by using the joint simulation approach, while the hierarchical approach will provide more inferred ore tonnage, thus a more conservative classification. In other words, the joint simulation approach reduces the uncertainty in the resources model by a more judicious use of the drill hole information.

5. Conclusions

Up until now, the joint simulation of grade and rock type has been restricted to a stationary setting, which is questionable when the spatial layout of rock type domains exhibits spatial trends. This paper extends such a simulation to a non-stationary setting, by assuming that the rock type is obtained by truncating an IRF- k. Tools and algorithms have been presented for inferring the model parameters and constructing realizations conditioned to existing data. In practice, the main difficulty is the identification of the joint spatial correlation structure, for which a semi-automated procedure has been designed, based on a least-squares fitting of the indicator covariance and cross-covariance between all the pairs of data locations. This procedure can be subject to further improvements, so as to reduce the number of subjective decisions of the modeler and to enhance the effectiveness of the optimization algorithms when a large number of parameters have to be fitted.

The proposed tools and algorithms have been applied to a porphyry copper deposit, where the copper grade and rock type have been jointly simulated conditionally to the information at drill hole samples. This case study has proven the capability of the proposed model and algorithms to jointly simulate a grade and a rock type and to reproduce the behavior of the grade near the rock type boundary, as well as the spatial trend in the rock type distribution.

Acknowledgements

The authors are grateful to three anonymous reviewers for their constructive comments. The first author acknowledges the PiensaCobre student scholarship granted by Codelco-Chile and the Center for Mathematical Modeling at University of Chile. The second author acknowledges the support of the Chilean Commission for Scientific and Technological Research, through Project CONICYT PIA Anillo ACT1407.

References

Armstrong, M., Galli, A., Beucher, H., Le Loc'h, G., Renard, D., Doligez, B., Eschard, R., Geffroy, F., 2011. Plurigaussian Simulations in Geosciences. Springer, Berlin, p. 176.

Arroyo, D., Emery, X., 2016. Spectral simulation of vector random fields with stationary Gaussian increments in d-dimensional Euclidean spaces. Stoch. Environ. Res. Risk Assess., pp. 1–10. http://dx.doi.org/10.1007/s00477-016-1225-7.

Chilès, J.P., Delfiner, P., 2012. Geostatistics: Modeling Spatial Uncertainty. Wiley, Hoboken, New Jersey, p. 699.

Dimitrakopoulos, R., Luo, X., 2004. Generalized sequential Gaussian simulation on group size ν and screen-effect approximations for large field simulations. Math. Geol. 36 (5), 567–590.

Dowd, P.A., 1997. Structural controls in the geostatistical simulation of mineral deposits. In: Baafi, E.Y., Schofield, N.A. (Eds.), Geostatistics Wollongong'96. Kluwer Academic, Dordrecht, The Netherlands, pp. 647–657.

Emery, X., Arroyo, D., Peláez, M., 2014. Simulating large Gaussian vectors subject to inequality constraints by Gibbs sampling. Math. Geosci. 46, 265–283.

Emery, X., Arroyo, D., Porcu, E., 2016. An improved spectral turning-bands algorithm for simulating stationary vector Gaussian random fields. Stoch. Environ. Res. Risk Assess. 30 (7), 1863–1873.

Emery, X., Silva, D.A., 2009. Conditional co-simulation of continuous and categorical variables for geostatistical applications. Comput. Geosci. 35 (6), 1234–1246.

Frikken, P., 2003. Breccia-hosted Copper-molybdenum Mineralisation at Rio Blanco, Chile. PhD Dissertation. University of Tasmania, Hobart, Australia, p. 290.

Gneiting, T., Ševčíková, H., Percival, D.B., Schlather, M., Jiang, Y., 2006. Fast and exact simulation of large Gaussian lattice systems in R^2: exploring the limits. J. Comput. Graph. Stat. 15 (3), 483–501.

Goovaerts, P., 2001. Geostatistical modelling of uncertainty in soil science. Geoderma 103 (1–2), 3–26.

Lantuéjoul, C., 2002. Geostatistical Simulation: Models and Algorithms. Springer-Verlag, Berlin, Germany, p. 256.

Liang, M., Marcotte, D., Shamsipour, P., 2016. Simulation of non-linear coregionalization models by FFTMA. Comput. Geosci. 89, 220–231.

Madani, N., Emery, X., 2017. Plurigaussian modeling of geological domains based on the truncation of non-stationary Gaussian random fields. Stoch. Environ. Res. Risk Assess. 31 (4), 893–913.

Maleki, M., Emery, X., 2015. Joint simulation of grade and rock type in a stratabound copper deposit. Math. Geosci. 47, 471–495.

Roldão, D., Ribeiro, D., Cunha, E., Noronha, R., Madsen, A., Masetti, L., 2012. Combined use of lithological and grade simulations for risk analysis in iron ore, Brazil. In: Abrahamsen, P., Hauge, R., Kolbjørnsen, O. (Eds.), Geostatistics Oslo 2012. Springer, Berlin, Germany, pp. 423–434.

Yuan, Y., 2015. Recent advances in trust region algorithms. Math. Program. 151 (1), 249–281.